Stimulated Raman Scattering Imposes Fundamental Limits to the Duration and Bandwidth of Temporal Cavity Solitons

Yadong Wang,* Miles Anderson,† Stéphane Coen, Stuart G. Murdoch, and Miro Erkintalo‡
The Dodd-Walls Centre for Photonic and Quantum Technologies, Department of Physics, The University of Auckland, Auckland 1142, New Zealand

(Received 1 September 2017; revised manuscript received 13 November 2017; published 31 January 2018)

Temporal cavity solitons (CS) are optical pulses that can persist in passive resonators, and they play a key role in the generation of coherent microresonator frequency combs. In resonators made of amorphous materials, such as fused silica, they can exhibit a spectral redshift due to stimulated Raman scattering. Here we show that this Raman-induced self-frequency-shift imposes a fundamental limit on the duration and bandwidth of temporal CSs. Specifically, we theoretically predict that stimulated Raman scattering introduces a previously unidentified Hopf bifurcation that leads to destabilization of CSs at large pump-cavity detunings, limiting the range of detunings over which they can exist. We have confirmed our theoretical predictions by performing extensive experiments in synchronously driven fiber ring resonators, obtaining results in excellent agreement with numerical simulations. Our results could have significant implications for the future design of Kerr frequency comb systems based on amorphous microresonators.

DOI: 10.1103/PhysRevLett.120.053902

Temporal cavity solitons (CSs) are pulses of light that can circulate indefinitely in passive driven nonlinear resonators. They were first observed and studied in macroscopic fiber ring cavities, and proposed as ideal candidates for bits in all-optical buffers [1–4]. More recently, they have also been observed in monolithic microresonators [5–8], where they play a central role in the generation of stable, low noise, wide bandwidth optical frequency combs [9–11].

Temporal CSs can persist without changes in their shape or energy thanks to a delicate double balance [12]. The material Kerr nonlinearity compensates for the solitons' dispersive spreading, while all energy they lose is replenished through interactions with the continuous wave (cw) field driving the cavity. In addition to these fundamental interactions, the characteristics of temporal CSs can be influenced by "higher-order" perturbations, such as higher-order dispersion [13,14] or avoided mode crossings [15]. In resonators made of amorphous materials, such as silica glass, an effect of particular significance is stimulated Raman scattering (SRS), which causes temporal CSs to be spectrally redshifted relative to the driving wavelength [8,16–18]. Signatures of such CS self-frequency shift were first observed in the context of frequency comb generation in silicon nitride microresonators [17], and subsequently in experiments using silica wedge resonators [7] and silica microspheres [8]. Indirect time domain signatures have also been reported in macroscopic fiber ring resonators [19].

In addition to shifting the CS center frequency, SRS can also impact on the range of CS existence. Indeed, in a pioneering theoretical work [16], Milián *et al.* observed that, in the presence of SRS, temporal CSs may not exist over the entire range of parameters where they are expected to do so in the absence of SRS. Yet, the precise fashion in which SRS affects the existence and stability of CSs has not to date been thoroughly investigated, and to the best of our knowledge, no experimental studies have been reported that would demonstrate the impact of SRS on CS existence.

In this Letter, we theoretically and experimentally demonstrate that SRS can significantly restrict the range of CS existence. In particular, we show that, due to SRS, CSs undergo a previously unidentified Hopf bifurcation at large cavity detunings, leading to instability dynamics that limit the range of parameters over which they can stably exist. We show that this new instability sets a fundamental limit for the minimum duration that a CS can possess for given resonator parameters, thereby setting an upper limit for the frequency comb bandwidth that can be achieved. We have confirmed our theoretical predictions by performing extensive experiments in three different fiber ring resonators.

We begin by theoretically analyzing the impact of SRS on the existence and stability of temporal CSs. To this end, we analyze the generalized mean-field Lugiato-Lefever equation (LLE) [20–22] that includes the delayed Raman nonlinearity [8,16,17]. We write the equation in dimensionless form, assuming anomalous group-velocity dispersion (for normalization, see Supplemental Material [23]):

$$\frac{\partial E(t,\tau)}{\partial t} = \left(-1 - i\Delta + i\frac{\partial^2}{\partial \tau^2}\right)E + S + i[(1-f_R)|E|^2 + f_R[\Gamma(\tau,\tau_s) \otimes |E|^2]]E. \quad (1)$$

Here, the variable t describes the *slow* evolution of the intracavity field $E(t,\tau)$ at the scale of the cavity photon

lifetime, while τ is a *fast* time variable defined in a comoving reference frame that describes the field's temporal profile over a single round trip. The terms on the right-hand side of Eq. (1) describe, respectively, cavity losses, cavity phase detuning, group-velocity dispersion, external driving, instantaneous Kerr nonlinearity, and the delayed Raman nonlinearity, with $\otimes$ denoting convolution. The Raman response of the resonator is described by the Raman fraction f_R as well as the normalized response function $\Gamma(\tau,\tau_s)$, which is related to the usual time-domain Raman response function $h_R(\tau)$ [24] through $\Gamma(\tau,\tau_s)=\tau_s h_R(\tau\tau_s)$, where the normalization time scale $\tau_s=\sqrt{|\beta_2|L/(2\alpha)}$, with $\beta_2<0$ the resonator's group-velocity dispersion coefficient, L the resonator round trip length, and α half the fraction of power lost per round trip (the cavity finesse $\mathcal{F}=\pi/\alpha$). In the calculations that follow, we will assume a silica glass resonator for which $f_R\approx 0.18$ and the form of the response function is well known [24,25].

In the absence of SRS ($f_R=0$), the dynamics and solutions of Eq. (1) are governed by the cavity detuning Δ and driving strength S [26]. SRS introduces, however, an additional dependency on the normalization time scale τ_s. This can be understood by recalling that the impact of SRS depends on the physical durations (and bandwidths) of the intracavity field features, with shorter CSs (associated with smaller values of τ_s) more strongly affected.

To illustrate how SRS affects the stability and existence of CSs, we show in Fig. 1(a) the steady-state CS solutions of Eq. (1) for a constant driving power $X=|S|^2=130$ in the presence ($f_R=0.18$, red curve) and absence ($f_R=0$, blue curve) of SRS. Also shown are temporal [Fig. 1(b)] and spectral [Fig. 1(c)] profiles for a CS at a typical

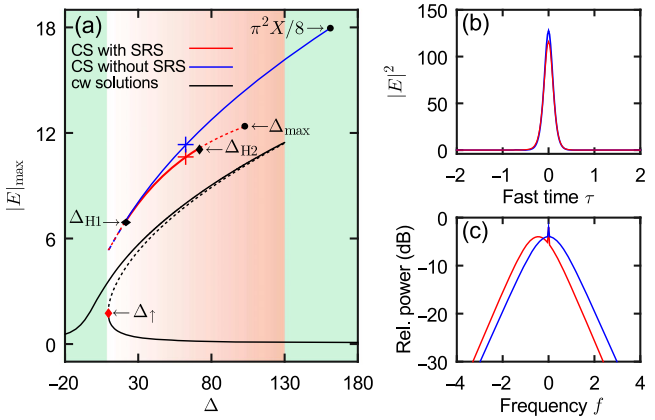

FIG. 1. (a) Peak amplitude of the intracavity field, $|E|_{max}$, as a function of cavity detuning Δ for $X=130$. Black curves represent cw solutions, while red and blue curves show CS solutions with and without SRS, respectively. The dashed curves correspond to unstable solutions. (b) Temporal and (c) spectral CS profiles for $\Delta=62$. The colors match those used in (a). The corresponding solutions are marked with crosses in (a). The green and red shaded areas in (a) indicate regions of monostability and bistability of the cw solutions, respectively.

detuning $\Delta=62$. The solutions were obtained by finding the time-localized solutions of Eq. (1) using a continuation scheme based on the Newton-Raphson method [21]; a normalization time scale $\tau_s=1.9$ ps (corresponding to one of the experiments that will follow) was used for calculations when including SRS. We also show in Fig. 1(a) the steady-state cw solutions (black curves) of Eq. (1). The cw solutions exhibit pronounced bistability, with the middle branch being unconditionally unstable (dashed black curve).

For small detunings, SRS does not significantly perturb the CS solutions: in both cases (with and without SRS), the solutions exist for detunings above the up-switching point $\Delta_\uparrow$, exhibit well-known unstable behaviors for small detunings (dashed blue and red curves) [27–30], and become stable through an inverse Hopf bifurcation (Δ_{H1}) as the detuning increases. However, as Δ increases further, we see a distinct deviation between the solutions obtained in the presence and absence of SRS. This can be understood by noting that the duration of a CS scales inversely with $\sqrt{\Delta}$ [21]: for large detunings the CSs are temporally narrower, and hence spectrally broader, resulting in stronger overlap with the Raman gain spectrum.

In the presence of SRS, CSs exhibit lower peak powers, longer durations, and their center frequency is downshifted [cf. Figs. 1(b) and 1(c)]. But in addition to perturbing their characteristics, it is evident from Fig. 1(a) that SRS also impacts on their range of stability and existence. In particular, we find that, in the presence of SRS, CSs can undergo a second Hopf bifurcation at large detunings [denoted as Δ_{H2} in Fig. 1(a)], leading to unstable dynamics. We suspect this instability arises physically because the solitons' decreasing temporal duration gives rise to a more pronounced frequency downshift from the driving frequency. Such a frequency shift can be envisaged to perturb the solitons' energy balance, and eventually cause them to wholly lose their entrainment to the driving field.

Dynamical (split-step) simulations of Eq. (1) reveal that the previously unidentified, large-Δ *unstable* CSs, exhibit behaviors qualitatively similar to those observed for unstable CSs below the first Hopf bifurcation point Δ_{H1} [28,29]: for detunings slightly above Δ_{H2}, the CSs exhibit oscillatory behavior, but as Δ increases further, they experience an abrupt collapse to the cw state (see Supplemental Material [23]). The simulations further show that, in the region where persistently oscillating CSs exist, the period and depth of the oscillations depend nontrivially on the parameters Δ and X (see Supplemental Material [23]). Furthermore, all the persistent oscillations we have found so far are associated with a single frequency; no period-doubling or chaotic behaviors have been found.

The results in Fig. 1(a) also show that, in the presence of SRS, the CS solutions cease to exist altogether at a detuning significantly smaller [Δ_{max} in Fig. 1(a)] than the theoretical limit of $\pi^2X/8$ observed in the absence of SRS [31]. We emphasize, however, that Δ_{max} only represents a theoretical

upper limit of CS existence: in practice CSs cannot be sustained for detunings far above Δ_{H2} because of the nature of the instability dynamics (see Supplemental Material [23]). At this point, we also emphasize that the large-Δ instability regime uncovered in Fig. 1(a) was not discussed in Ref. [16]. In fact, we have carefully verified that the parameters used in Ref. [16] are such that the second Hopf bifurcation does not manifest itself. The CS instabilities studied in Ref. [16] are rather those occurring for detunings below the first Hopf bifurcation point Δ_{H1}.

The precise detunings Δ_{H2} and Δ_{max} depend on the normalization time scale τ_s and the driving power X. To gain more insight, we evaluated the CS branches as a function of Δ [as in Fig. 1(a)] for a wide range of τ_s and X, and extracted Δ_{H2} and Δ_{max} for each set of parameters. Figure 2(a) summarizes our findings. Here we show Δ_{H2} (blue curves) and Δ_{max} (red curves) as a function of X for five different values of τ_s. The parameter boundaries, between which CSs can exist in the absence of SRS [28], are also displayed (black curves).

For small driving powers X (and/or large normalization time scales τ_s), we observe no secondary Hopf bifurcation and the upper limit of CS existence follows closely the expected value of $\pi^2 X/8$. However, for larger driving powers (and/or shorter normalization time scales τ_s), we see the appearance of the second Hopf bifurcation at large Δ, and we find that the upper limit of CS existence is significantly reduced from the Raman-free values. Surprisingly, while that upper limit Δ_{max} monotonically increases with the driving power X, the upper limit of CS stability (determined by Δ_{H2}) does not. Instead, we find that immediately after the first appearance of the second Hopf, the bifurcation point Δ_{H2} exhibits a small *decline* with increasing X, but eventually saturates to an almost constant value $\Delta_{H2S} = \lim_{X\gg 1} \Delta_{H2}$ that depends only on the normalization time scale τ_s.

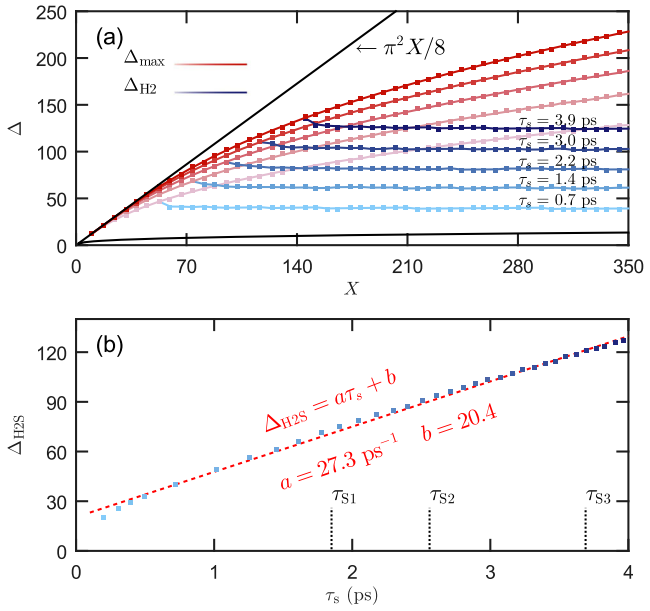

FIG. 2. (a) Cavity detunings Δ_{H2} and Δ_{max}, where the CS solution loses its stability (blue markers) and ceases to exist (red markers), respectively, as a function of driving power X and for a variety of τ_s. The squares correspond to simulated points, while the solid curves are a guide to the eye. Black curves indicate limits of CS existence in the absence of SRS. (b) Saturated limit detuning $\Delta_{H2S} = \lim_{X\gg 1} \Delta_{H2}$ as a function of the normalization time scale τ_s. Dashed red curve shows a linear fit. The three values of τ_s realized in our experiments are highlighted at the bottom of (b).

The results in Fig. 2(a) suggest that, because of SRS, there exists a maximum detuning Δ_{H2S} above which CSs can no longer remain stable in a given resonator, regardless of the driving power. Furthermore, due to the nature of the instability dynamics, this detuning also approximates well the upper limit of practical CS existence. As alluded to in Fig. 2(a), Δ_{H2S} depends almost exclusively on the resonator parameters through the normalization time scale τ_s, and in Fig. 2(b), we plot Δ_{H2} as a function of τ_s. As can be seen, the dependence is quasilinear, and only becomes nonlinear for very small $\tau_s < 0.5$ ps.

The observation that SRS imposes an upper limit for CS detunings also implies a lower limit for their temporal durations. Indeed, the duration of a temporal CS is approximately given by $\tau_0 = \tau_s/\sqrt{\Delta}$ [1,5,21]. Thus, in the presence of SRS, the minimum duration that a (stable) CS can possess is $\tau_{min} \approx \tau_s/\sqrt{\Delta_{H2S}}$. For $\tau_s > 0.5$ ps we can approximate [cf. Fig. 2(b)]

$$\tau_{min} = \frac{\tau_s}{\sqrt{a\tau_s + b}}, \tag{2}$$

where $a = 27.3$ ps^{-1} and $b = 20.4$ are extracted from the linear fit shown in Fig. 2(b). This simple linear approximation can be used to estimate the minimum (maximum) CS duration (bandwidth) achievable in silica resonators. (For other amorphous resonators, the coefficients a and b will likely be different.) We have carefully verified that this result is consistent with prior experimental reports of CSs in various silica resonators [2,7,8,13].

To test our theoretical predictions, we have performed experiments using synchronously driven macroscopic fiber ring resonators, with an overall setup similar to the one used in [19]. Three different resonators were used so as to examine the effect of different normalization time scales τ_s. The resonators are all made up of single-mode optical fiber laid in a ring configuration and closed on themselves by a 95/5 coupler. Each of them also incorporates a 99/1 tap coupler through which the intracavity dynamics can be monitored in real time.

Because the resonators contain no other elements, they display very high finesse $\mathcal{F}$. This allows us to reach high values of normalized driving power $X \propto \mathcal{F}^3$, as required

for the study of SRS-induced limits of CS existence [see Fig. 2(a)]. To study the effect of the normalization time scale τ_s, our three different cavities have different round trip lengths of $L_1 = 13$ m, $L_2 = 25$ m, and $L_3 = 50$ m and finesses $\mathcal{F}_1 = 77$, $\mathcal{F}_2 = 77$, and $\mathcal{F}_3 = 69$; the corresponding normalization time scales are $\tau_{S1} = 1.9$ ps, $\tau_{S2} = 2.6$ ps, and $\tau_{S3} = 3.7$ ps, respectively.

We drive our cavities with flattop nanosecond pulses whose repetition rate is synchronized to the respective cavity round trip time [19,32,33]. These pump pulses have a duration of 1.2 ns, and they are generated by modulating the output of a narrow linewidth cw laser with a 12 GHz intensity modulator. Before the pulses are injected into the cavity, they are amplified using an Erbium-doped fiber amplifier, and spectrally filtered to remove amplified spontaneous emission. Together with the high cavity finesse, this pumping method allows us to achieve high normalized driving powers up to $X \approx 200$.

To experimentally study the limits of CS existence, we linearly tune the cw laser frequency so as to continuously scan the cavity detuning across individual resonances. By simultaneously measuring the cavity output (extracted by the 1% tap coupler) with a fast 12.5 GHz photodetector, we can monitor the intracavity dynamics in real time. This allows us to observe the creation and annihilation of CSs as the detuning is scanned [34], and from the acquired data, we can extract their limits of existence.

Figure 3(a) shows an example of the measured intracavity dynamics as the cavity detuning Δ is linearly scanned from 0 to 110 (corresponding to 6.3×10^{-4} rad/roundtrip) at a constant driving power $X = 130$ (~11.3 W peak power). For low detunings the field corresponds to an extended modulation instability pattern which is visible in Fig. 3(a) as a solid bright band [35]. Out of this chaotic signal, CSs emerge as the detuning increases above $\Delta \approx 30$. The CSs exhibit curved trajectories as the detuning increases, which is a known effect of SRS [19]. When the detuning reaches $\Delta_{\mathrm{lim}} \approx 101$, all the CSs disappear almost simultaneously. (Small discrepancies are attributed to inhomogeneities in the pump pulse profile.) Accordingly, this corresponds to the limit detuning beyond which solitons can no longer be sustained. The observed value is significantly smaller than the theoretical limit $\pi^2 X/8 \approx 160$ expected without SRS.

To more comprehensively test our theoretical predictions, we have repeated the above experiment for a wide range of driving powers X and using all three of our resonators to sample different normalization time scales τ_s. For each experiment, we perform a detuning scan [as in Fig. 3(a)], and extract the limit detuning beyond which CSs no longer exist. Our experimental findings are summarized in Fig. 3(b). Here the circle markers correspond to experimental data acquired for the different cavities, while the dashed curves show results from numerical simulations of the LLE (the simulations use experimental parameters). We estimate the error in our measured limit detunings to be

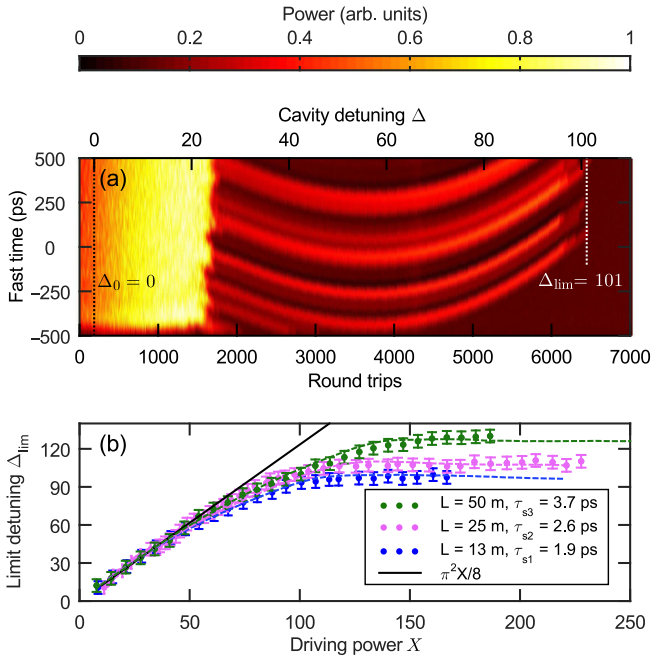

FIG. 3. (a) Intracavity dynamics as the detuning is scanned from 0 to 110 (top x axis) during about 7000 round trips (bottom x axis) with $X \approx 130$. The cavity is 13 m long and has a normalization time scale $\tau_{S1} = 1.9$ ps. Dashed black and white vertical lines indicate zero detuning and the limit detuning Δ_{lim} at which CSs cease to exist, respectively. (b) Limit detuning Δ_{lim} at which CSs cease to exist as a function of driving power X and for three different normalization time scales τ_s. The circle markers are extracted from experiments, while the dashed curves correspond to results from numerical simulations of the LLE. The solid black line shows the theoretical CS existence limit in the absence of SRS, i.e., $\Delta_{\mathrm{max}} = \pi^2 X/8$.

about ± 5, arising predominantly from inhomogeneities in the pump pulse profile and imprecision in extracting the zero-detuning reference. As can be seen, our numerical simulations are in excellent agreement with experimental findings. Furthermore, in agreement with our theoretical predictions [see Fig. 2(a)], the limit detuning Δ_{lim} initially increases with X, but eventually saturates to a constant value. This saturation occurs in all of our resonators but results in different saturated limit detunings due to the different normalization time scales τ_s. Overall, these measurements confirm our main hypotheses: SRS limits the range of CS existence, and gives rise to a maximum detuning beyond which CSs cannot exist in a given resonator.

The experimental results in Fig. 3(b) are in excellent qualitative agreement with the theoretical findings in Fig. 2. However, careful analysis shows that our experiments consistently overestimate the upper limit of CSs existence compared to the theoretically predicted second Hopf bifurcation point Δ_{H2}. This discrepancy arises predominantly because the detuning is continuously increasing in our experiments. Indeed, the CSs persist briefly even after passing the second Hopf bifurcation point Δ_{H2}, and so a

continuously increasing detuning naturally leads to overestimation of their existence range. We have confirmed this hypothesis by performing additional experiments where the detuning is initially scanned and then stopped at different points close to the CS existence limit. Results are summarized in the Supplemental Material [23]: they demonstrate that the second Hopf bifurcation point Δ_{H2} reasonably approximates the practical upper limit of CS existence.

In conclusion, we have shown that, due to SRS, temporal CSs can lose their stability through a previously unidentified Hopf bifurcation that occurs for large detunings. Furthermore, we have shown that this instability gives rise to a maximum detuning above which stable CSs cannot exist in a given resonator, regardless of the driving power. We have confirmed our theoretical analysis through comprehensive experiments in three different fiber ring resonators. In addition to unveiling a new type of CS instability, our results could impact the design of frequency comb generators based on microresonators where SRS plays a role, such as silica microspheres [8], wedge resonators [36], and fiber-based Fabry-Perot resonators [37].

We acknowledge support from the Marsden Fund of the Royal Society of New Zealand. M. E. further acknowledges support from the Rutherford Discovery Fellowships of the Royal Society of New Zealand. Y. W. acknowledges support from the Dodd-Walls Centre for Photonic and Quantum Technologies.

*ywan505@aucklanduni.ac.nz
†Present address: École Polytechnique Fédérale de Lausanne (EPFL), CH-1015 Lausanne, Switzerland.
‡m.erkintalo@auckland.ac.nz

[1] S. Wabnitz, Suppression of interactions in a phase-locked soliton optical memory, Opt. Lett. **18**, 601 (1993).
[2] F. Leo, S. Coen, P. Kockaert, S.-P. Gorza, P. Emplit, and M. Haelterman, Temporal cavity solitons in one-dimensional Kerr media as bits in an all-optical buffer, Nat. Photonics **4**, 471 (2010).
[3] J. K. Jang, M. Erkintalo, S. G. Murdoch, and S. Coen, Writing and erasing of temporal cavity solitons by direct phase modulation of the cavity driving field, Opt. Lett. **40**, 4755 (2015).
[4] J. K. Jang, M. Erkintalo, J. Schröder, B. J. Eggleton, S. G. Murdoch, and S. Coen, All-optical buffer based on temporal cavity solitons operating at 10 Gb/s, Opt. Lett. **41**, 4526 (2016).
[5] T. Herr, V. Brasch, J. D. Jost, C. Y. Wang, N. M. Kondratiev, M. L. Gorodetsky, and T. J. Kippenberg, Temporal solitons in optical microresonators, Nat. Photonics **8**, 145 (2014).
[6] X. Xue, Y. Xuan, Y. Liu, P.-H. Wang, S. Chen, J. Wang, D. E. Leaird, M. Qi, and A. M. Weiner, Mode-locked dark pulse Kerr combs in normal-dispersion microresonators, Nat. Photonics **9**, 594 (2015).
[7] X. Yi, Q.-F. Yang, K. Y. Yang, M.-G. Suh, and K. Vahala, Soliton frequency comb at microwave rates in a high-Q silica microresonator, Optica **2**, 1078 (2015).
[8] K. E. Webb, M. Erkintalo, S. Coen, and S. G. Murdoch, Experimental observation of coherent cavity soliton frequency combs in silica microspheres, Opt. Lett. **41**, 4613 (2016).
[9] P. Del'Haye, T. Herr, E. Gavartin, M. L. Gorodetsky, R. Holzwarth, and T. J. Kippenberg, Octave Spanning Tunable Frequency Comb from a Microresonator, Phys. Rev. Lett. **107**, 063901 (2011).
[10] T. J. Kippenberg, R. Holzwarth, and S. A. Diddams, Microresonator-based optical frequency combs, Science **332**, 555 (2011).
[11] P. Del'Haye, A. Coillet, T. Fortier, K. Beha, D. C. Cole, K. Y. Yang, H. Lee, K. J. Vahala, S. B. Papp, and S. A. Diddams, Phase-coherent microwave-to-optical link with a self-referenced microcomb, Nat. Photonics **10**, 516 (2016).
[12] N. N. Akhmediev and A. Ankiewicz, Dissipative solitons, Lect. Notes Phys. **661**, 1 (2005).
[13] J. K. Jang, M. Erkintalo, S. G. Murdoch, and S. Coen, Observation of dispersive wave emission by temporal cavity solitons, Opt. Lett. **39**, 5503 (2014).
[14] Y. Wang, F. Leo, J. Fatome, M. Erkintalo, S. G. Murdoch, and S. Coen, Universal mechanism for the binding of temporal cavity solitons, Optica **4**, 855 (2017).
[15] T. Herr, V. Brasch, J. D. Jost, I. Mirgorodskiy, G. Lihachev, M. L. Gorodetsky, and T. J. Kippenberg, Mode Spectrum and Temporal Soliton Formation in Optical Microresonators, Phys. Rev. Lett. **113**, 123901 (2014).
[16] C. Milián, A. V. Gorbach, M. Taki, A. V. Yulin, and D. V. Skryabin, Solitons and frequency combs in silica microring resonators: Interplay of the Raman and higher-order dispersion effects, Phys. Rev. A **92**, 033851 (2015).
[17] M. Karpov, H. Guo, A. Kordts, V. Brasch, M. H. P. Pfeiffer, M. Zervas, M. Geiselmann, and T. J. Kippenberg, Raman Self-Frequency Shift of Dissipative Kerr Solitons in an Optical Microresonator, Phys. Rev. Lett. **116**, 103902 (2016).
[18] Q.-F. Yang, X. Yi, K. Y. Yang, and K. Vahala, Stokes solitons in optical microcavities, Nat. Phys. **13**, 53 (2017).
[19] M. Anderson, Y. Wang, F. Leo, S. Coen, M. Erkintalo, and S. G. Murdoch, Super Cavity Solitons and the Coexistence of Multiple Nonlinear States in a Tristable Passive Kerr Resonator, Phys. Rev. X **7**, 031031 (2017).
[20] L. A. Lugiato and R. Lefever, Spatial Dissipative Structures in Passive Optical Systems, Phys. Rev. Lett. **58**, 2209 (1987).
[21] S. Coen, H. G. Randle, T. Sylvestre, and M. Erkintalo, Modeling of octave-spanning kerr frequency combs using a generalized mean-field Lugiato-Lefever model, Opt. Lett. **38**, 37 (2013).
[22] Y. K. Chembo and C. R. Menyuk, Spatiotemporal Lugiato-Lefever formalism for Kerr-comb generation in whispering-gallery-mode resonators, Phys. Rev. A **87**, 053852 (2013).
[23] See Supplemental Material at http://link.aps.org/supplemental/10.1103/PhysRevLett.120.053902 for additional results on the CS instability dynamics and normalization of the model equation.
[24] R. H. Stolen, J. P. Gordon, W. J. Tomlinson, and H. A. Haus, Raman response function of silica-core fibers, J. Opt. Soc. Am. B **6**, 1159 (1989).

[25] D. Hollenbeck and C. D. Cantrell, Multiple-vibrational-mode model for fiber-optic Raman gain spectrum and response function, J. Opt. Soc. Am. B **19**, 2886 (2002).
[26] S. Coen and M. Erkintalo, Universal scaling laws of Kerr frequency combs, Opt. Lett. **38**, 1790 (2013).
[27] M. Erkintalo, G. Genty, B. Wetzel, and J. M. Dudley, Limitations of the linear raman gain approximation in modeling broadband nonlinear propagation in optical fibers, Opt. Express **18**, 25449 (2010).
[28] F. Leo, L. Gelens, P. Emplit, M. Haelterman, and S. Coen, Dynamics of one-dimensional Kerr cavity solitons, Opt. Express **21**, 9180 (2013).
[29] M. Anderson, F. Leo, S. Coen, M. Erkintalo, and S. G. Murdoch, Observations of spatiotemporal instabilities of temporal cavity solitons, Optica **3**, 1071 (2016).
[30] M. Yu, J. K. Jang, Y. Okawachi, A. G. Griffith, K. Luke, S. A. Miller, X. Ji, M. Lipson, and A. L. Gaeta, Breather soliton dynamics in microresonators, Nat. Commun. **8**, 14569 (2017).
[31] I. V. Barashenkov and Y. S. Smirnov, Existence and stability chart for the ac-driven, damped nonlinear Schrödinger solitons, Phys. Rev. E **54**, 5707 (1996).
[32] S. Coen and M. Haelterman, Modulational Instability Induced by Cavity Boundary Conditions in a Normally Dispersive Optical Fiber, Phys. Rev. Lett. **79**, 4139 (1997).
[33] F. Copie, M. Conforti, A. Kudlinski, A. Mussot, and S. Trillo, Competing Turing and Faraday Instabilities in Longitudinally Modulated Passive Resonators, Phys. Rev. Lett. **116**, 143901 (2016).
[34] K. Luo, J. K. Jang, S. Coen, S. G. Murdoch, and M. Erkintalo, Spontaneous creation and annihilation of temporal cavity solitons in a coherently driven passive fiber resonator, Opt. Lett. **40**, 3735 (2015).
[35] M. Haelterman, S. Trillo, and S. Wabnitz, Dissipative modulation instability in a nonlinear dispersive ring cavity, Opt. Commun. **91**, 401 (1992).
[36] X. Yi, Q.-F. Yang, K. Y. Yang, and K. Vahala, Theory and measurement of the soliton self-frequency shift and efficiency in optical microcavities, Opt. Lett. **41**, 3419 (2016).
[37] E. Obrzud, S. Lecomte, and T. Herr, Temporal solitons in microresonators driven by optical pulses, Nat. Photonics **11**, 600 (2017).